

Finding purifications with minimal entanglement

Johannes Hauschild,^{1,*} Eyal Leviatan,² Jens H. Bardarson,³ Ehud Altman,⁴ Michael P. Zaletel,⁵ and Frank Pollmann¹

¹*Department of Physics, T42, Technische Universität München,
James-Frank-Straße 1, D-85748 Garching, Germany*

²*Department of Condensed Matter Physics, Weizmann Institute of Science, Rehovot 7610001, Israel*

³*Department of Physics, KTH Royal Institute of Technology, Stockholm SE-10691, Sweden*

⁴*Department of Physics, University of California, Berkeley, CA 94720*

⁵*Department of Physics, Princeton University, Princeton, NJ 08540, USA*

Purification is a tool that allows to represent mixed quantum states as pure states on enlarged Hilbert spaces. A purification of a given state is not unique and its entanglement strongly depends on the particular choice made. Moreover, in one-dimensional systems, the amount of entanglement is linked to how efficiently the purified state can be represented using matrix-product states (MPS). We introduce an MPS based method that allows to find the minimally entangled representation by iteratively minimizing the second Renyi entropy. First, we consider the thermofield double purification and show that its entanglement can be strongly reduced especially at low temperatures. Second, we show that a slowdown of the entanglement growth following a quench of an infinite temperature state is possible.

Introduction. Simulating quantum many-body systems faces a fundamental difficulty due to the complexity required to represent highly entangled states. Significant progress has been made through the observation that quantum ground states of interest often have only limited (area law) entanglement, and thus can be represented efficiently using matrix-product states (MPS) [1–3] in one dimension (1D) and generalized tensor-product states [4] in higher dimensions. Such approaches have been particularly successful in the study of ground state properties of 1D systems, where the density matrix renormalization group (DMRG) method [5] revolutionized the efficiency of numerical methods.

To extend the success of DMRG to transport and non-equilibrium phenomena, it is necessary to simulate real-time evolution [6–8]. The bipartite entanglement of pure states generically grows linearly with time, which leads to a rapid exponential blow up in computational cost, limiting pure-state time evolution to rather short times. But while the entanglement growth limits the ability to compute the time evolution of pure quantum states, it need not impose the same restriction on mixed states [9]. It is then natural to ask if the time evolution of mixed states can be represented efficiently using MPS and what sets the difficulty of such computations.

There are different techniques for simulating mixed states using MPS methods, including a direct representation of the density matrix as a matrix product operator (MPO) [10], using minimally entangled typical thermal states (METTS) [11–13], and purification [14, 15]; in this paper we focus on the latter. In purification a density matrix ρ acting on a *physical* Hilbert space \mathcal{H}^P is represented as a pure state $|\psi\rangle$ in an enlarged space $\mathcal{H}^P \otimes \mathcal{H}^Q$:

$$\rho = \text{Tr}_Q |\psi\rangle \langle \psi|. \quad (1)$$

It is always sufficient to choose \mathcal{H}^Q to be identical to \mathcal{H}^P , “doubling” each degree of freedom (DoF) as il-

lustrated in Fig. 1(a). Formally, a purification can be found by diagonalizing the density matrix; in equilibrium this gives the thermofield double (TFD) purification, $|\psi_\beta\rangle = \frac{1}{\sqrt{Z}} \sum_n e^{-\beta E_n/2} |n\rangle_P |n\rangle_Q$, where $|n\rangle$ are the eigenvectors and E_n the eigenvalues of the Hamiltonian. It was recently argued that the TFD state can be efficiently represented with an MPS of bond dimension that grows at most polynomially with the inverse temperature [9]. The TFD is only one possible choice of purification, since Eq. (1) is left invariant under an arbitrary unitary transformation U_{anc} which acts only on the ancilla space \mathcal{H}^Q .

This gauge freedom may be used to reduce the entanglement in $|\psi\rangle$, rendering the MPS representation more efficient [16, 17]. Here, we propose a way to find the minimally entangled purification. This minimum defines the entanglement of purification E_p [18] [defined below in Eq. (2)], which thus plays a role similar to the entanglement entropy in the pure case: it bounds the bond dimension $\chi \geq e^{E_p}$ [19]. However, this lower bound is irrelevant unless there is an efficient algorithm to *find* the minimally entangled purification at a cost comparable to DMRG (e.g., $\mathcal{O}(\chi^3)$), which, since it constitutes a global optimization problem over the many-body Hilbert space, is not a priori obvious.

Below we introduce a method to find an approximately-optimal purification by sequentially applying local disentangling operations to the ancilla DoF. The cost of the disentangling procedure is comparable to DMRG, and the resulting entanglement \tilde{E}_p reproduces the known properties of E_p in certain limits. We use the method to optimize both the equilibrium purification and that of a time dependent state. We find that the method can significantly slow the entropy growth during real-time evolution down, as we demonstrate for both the transverse field Ising model and a disordered Heisenberg chain. For the latter, we find a

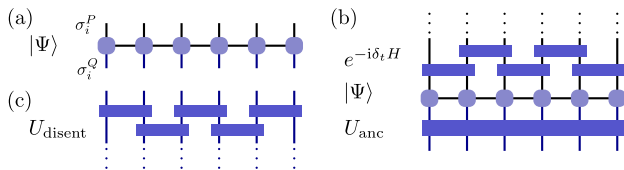


FIG. 1. (a) Schematic representation of purified states using MPS. (b) A purified state is evolved in real or imaginary time by acting on the physical degrees of freedom (e.g., using a Trotter decomposition of the time-evolution operator). The auxiliary degrees of freedom are only defined up to a global unitary U_{anc} which can be chosen to minimize the entanglement on the bonds. (c) The global U_{anc} is decomposed into a network of two-site gates to produce a disentangler U_{disent} .

slow spreading of \tilde{E}_p already for intermediate disorder strengths. In equilibrium, \tilde{E}_p approaches half of the entropy in the TFD state at low temperature.

Before proceeding we comment on the difference between the method presented here and two other proposals to compute long time dynamics efficiently using MPS. Some of us have shown recently that the dynamics of local quantities in thermalizing systems can be captured accurately using the time dependent variational principle (TDVP) [20], allowing to extract transport coefficients and even characteristics of chaos. Another one of us proposed a new truncation method to approximate the time evolution of a density matrix, represented as an MPO, to long times [21]. Both of these methods rely on the assumption that the increase of the non-local information encoded by the ever growing entanglement entropy is irrelevant to the evolution of observable properties in thermalizing systems. These methods attempt to simulate the correct macro-state rather than the nearly exact microstate. Thus the “truncation error” as usually defined in DMRG studies can be large as it is measured with respect to the exact state. In contrast, the approach presented here attempts, by optimizing the purification, to minimize the truncation error in order to compute the exact micro-state.

Purifications within the MPS formalism. To represent a purification as an MPS, we take $\mathcal{H}^P \sim \mathcal{H}^Q$ so that each “site” contains a doubled DoF. The purification then takes the standard MPS form with an enlarged local Hilbert space as shown in Fig. 1(a). At infinite temperature, the TFD purification is obtained by maximally entangling the physical and ancilla DoF on every site i , e.g., $|\psi_0\rangle = \prod_i \left(\frac{1}{\sqrt{d}} \sum_{\sigma_i} |\sigma_i\rangle_P |\sigma_i\rangle_Q \right)$, where σ_i runs over the local Hilbert space, resulting in a $\chi = 1$ MPS. In the standard purification approach, the finite temperature TFD is obtained from $|\psi_0\rangle$ using imaginary-time evolution, $|\psi_\beta\rangle \propto e^{-\frac{\beta}{2}H} |\psi_0\rangle$, from which thermal expectation values are evaluated as $\langle Y \rangle_\beta = \langle \psi_\beta | Y | \psi_\beta \rangle$. Here H acts only on \mathcal{H}^P . Similarly, to compute dy-

namical properties, for instance, $C(t, \beta) = \langle B^\dagger Y(t) B \rangle_\beta$, we define $|B(t, \beta)\rangle = e^{-itH} B |\psi_\beta\rangle$, so that $C(t, \beta) = \langle B(t, \beta) | Y | B(t, \beta) \rangle$. By taking $B = e^{i\epsilon X}$, this form is sufficient to find quantities of interest such as the spectral function $-i\partial_\epsilon C(t, \beta) = A_{YX}(t, \beta) = \langle [Y(t), X(0)] \rangle_\beta$. The requisite time evolution (both imaginary and real) can be simulated using standard methods [6–8, 22, 23].

The computational complexity of such simulations is generically linked to the bipartite von-Neumann entanglement entropy $S_{LL'} = -\text{Tr}(\rho_{LL'} \log(\rho_{LL'}))$, where $\rho_{LL'} = \text{Tr}_{RR'}(|\psi\rangle\langle\psi|)$ is the reduced density matrix defined by a bipartition $\mathcal{H}^P = L \otimes R$ and $\mathcal{H}^Q = L' \otimes R'$ at any of the bonds of the MPS; the bond dimension χ is bounded by $\chi \geq e^{S_{LL'}}$. Since other purifications can be obtained by acting with U_{anc} on the ancilla space, see Fig. 1(b), it is desirable to exploit this choice to reduce $S_{LL'}$. Karrasch et al. [16] noticed that a natural choice is the “backward time evolution,” $U_{\text{anc}} = e^{itH}$, because if B is local this choice leaves $|B(t, \beta)\rangle$ invariant outside the growing “light-cone” of the perturbation. Barthel [17] improved this approach by evolving both X and Y in the spectral function $A_{YX}(t, \beta) = \langle [Y(t), X(0)] \rangle_\beta = \langle [Y(t/2), X(-t/2)] \rangle_\beta$ as Heisenberg operators, which allows reaching times twice as long with comparable numerical effort [17, 24]. However, these prescriptions need not be optimal; ideally, we would minimize $S_{LL'}$ over all possible purifications, which would result in the entanglement of purification E_p [18]:

$$E_p[\rho_{LR}] \equiv \min_{|\psi\rangle} S_{LL'}[|\psi\rangle] = \min_{U_{\text{anc}}} S_{LL'}[U_{\text{anc}}|\psi\rangle]. \quad (2)$$

Equivalently, given an ansatz purification $|\psi\rangle$, we search for U_{anc} such that $U_{\text{anc}}|\psi\rangle$ has minimal entanglement; from this perspective U_{anc} is a “disentangling” operation.

We propose an algorithm to approximately identify the optimal U_{anc} via a sequence of local disentangling operations, producing a circuit $U_{\text{anc}} = U_{\text{disent}}$ of the form shown in Fig. 1(c): The time evolution is applied to the purified state using the time-evolving block-decimation algorithm (TEBD) [6]. This algorithm is based on a Trotter decomposition of the time-evolution operator e^{-itH} into two-site gates as illustrated in Fig. 1(b), which here act sequentially only on the physical DoF. During real-time evolution, we follow each Trotter step by acting with a row of disentangling two-site unitaries on the ancilla DoF. These two-site disentanglers can be found using an iterative scheme based on minimizing the second Renyi entropy as a cost function, similar to the optimizations of a multi-scale entanglement renormalization ansatz (MERA) [25]. During imaginary-time evolution we use slightly different, less local disentanglers; the details of the implementation are outlined in the Appendix. As the time evolution proceeds, we build up the disentangling unitary circuit U_{disent} . While the algorithm can suffer from numerical instabilities, we find empirically that it converges to a purification with significantly less entan-

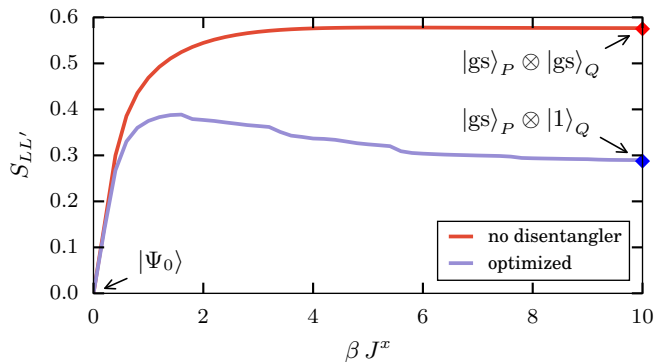


FIG. 2. Half-chain entanglement entropy of the finite temperature purification $|\psi_\beta\rangle \propto e^{-\frac{\beta}{2}H}|\psi_0\rangle$ in the generalized Ising model (3) with $L = 50$ sites, for the TFD state ($U_{\text{anc}} = \mathbb{1}$, upper line) and when disentangling up to 4 sites at once (lower line). The parameters $J^x = h^z = 1$ and $J^z = 0.1$ are chosen to be in the vicinity of the quantum phase transition. The diamonds on the right axis indicate the half-chain entanglement S_{gs} (blue) and $2S_{\text{gs}}$ (red) of the ground state $|\text{gs}\rangle$ obtained from DMRG.

lement compared to both backward time evolution and no disentangling at all. The method described above is particularly suitable for correlation functions which involve only a single purification, e.g., $C(t, \beta)$, as there is no need to keep track of U_{disent} . When two distinct purifications $|B(t)\rangle$ and $|A(t)\rangle$ are required, one would have to compress $U_{\text{disent}}^\dagger U_{\text{disent}}$ as a separate MPO.

Finite temperatures. To benchmark our algorithm, we study a concrete example, the generalized transverse field Ising model

$$H = -J^x \sum_{i=1}^{L-1} \sigma_i^x \sigma_{i+1}^x - J^z \sum_{i=1}^{L-1} \sigma_i^z \sigma_{i+1}^z - h^z \sum_{i=1}^L \sigma_i^z. \quad (3)$$

For $J^z = 0$, the model maps onto free fermions and exhibits a quantum phase transition at $h_c^z = J^x$. The term proportional to J^z introduces interactions and breaks integrability.

Figure 2 compares the entanglement of the optimized purification with the entanglement of the TFD state obtained by imaginary time evolution without disentangling, i.e., $U_{\text{anc}} = \mathbb{1}$. The infinite temperature state $|\psi_0\rangle$ has maximal entanglement between the physical and auxiliary DoF on each site, but no correlations between different sites, hence $S_{LL'} = 0$. For small β , the imaginary time evolution starts to build up correlations between neighboring sites, but it is not immediately possible to disentangle the state with a rotation in \mathcal{H}^Q . For example, a non-trivial unitary acting on σ_i^Q and σ_{i+1}^Q would lead to a strong correlation between σ_i^P and σ_{i+1}^P , and thus larger entanglement for a cut between sites i and $i+1$. However, due to the monogamy of entanglement, the build-up of quantum correlations between different sites insures the reduction of the entanglement between

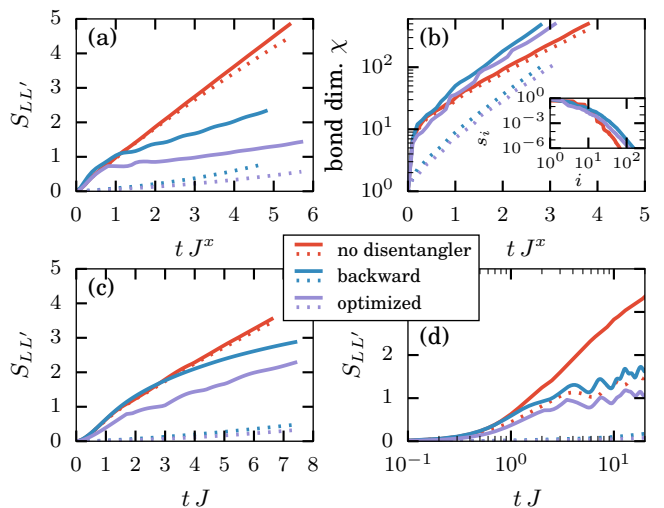


FIG. 3. Comparison of the entanglement in the purification state $|S_{L/2}^+(t, \beta = 0)\rangle = e^{-itH} S_{L/2}^+ |\psi_0\rangle$ for the Ising chain (3) with $L = 40$ sites, $J^x = h^z = 1$, $J^z = 0.1$ (a), and the Heisenberg chain (4) with $L = 80$ sites without disorder ($W = 0$) (c) and for a single disorder realization with $W = 5J$ (d). Panel (b) shows for the Ising model the MPS bond dimension required to keep $\langle S_{L/2,ex}^+(t) | S_{L/2}^+(t) \rangle \geq 1 - 10^6$, where $|S_{L/2,ex}^+(t)\rangle$ was obtained by a quasi-exact simulation discarding only Schmidt values $\leq 10^{-12}$. The inset in (b) shows the decay of the Schmidt values s_i on the central bond at time $tJ^x = 2$. In all panels, different colors compare different disentanglers. Solid lines show the maximum over all bonds, dotted lines show the mean over all bonds.

the physical and auxiliary spaces. Consequently, the disentangler can reduce the entanglement at larger β . This is most evident in the limit of large β in which $e^{-\frac{\beta}{2}H}$ becomes a projector $|\text{gs}\rangle \langle \text{gs}|$ onto the ground state $|\text{gs}\rangle$. In this limit the TFD purification ends up with two copies $|\text{gs}\rangle_P \otimes |\text{gs}\rangle_Q$ of the ground state in \mathcal{H}^P and \mathcal{H}^Q . In contrast, a perfect disentangling algorithm should be able to rotate $|\text{gs}\rangle_Q$ into an unentangled product state $|1\rangle_Q$, ending up with the state $|\text{gs}\rangle_P \otimes |1\rangle_Q$ which has only half as much entanglement as the TFD. The fact that we find a purification with an entanglement close to that of the ground state shows that our algorithm can indeed find the minimum, i.e., it finds E_p . Notably, we also find a maximum at intermediate β (although our algorithm suffers from numerical instabilities in this region). This can be understood from the fact that the entanglement of purification has contributions from both quantum fluctuations and thermal fluctuations, and the latter vanish for $\beta \rightarrow \infty$. A similar maximum is also present in the holographic prescription for the entanglement of purification [26, 27].

Real time evolution at infinite temperature.

Next, we consider the time evolution of a local operator applied to the infinite-temperature purification $|S_{L/2}^+(t, \beta = 0)\rangle = e^{-itH} S_{L/2}^+ |\psi_0\rangle$, where $S_i^+ = S_i^x + iS_i^y$.

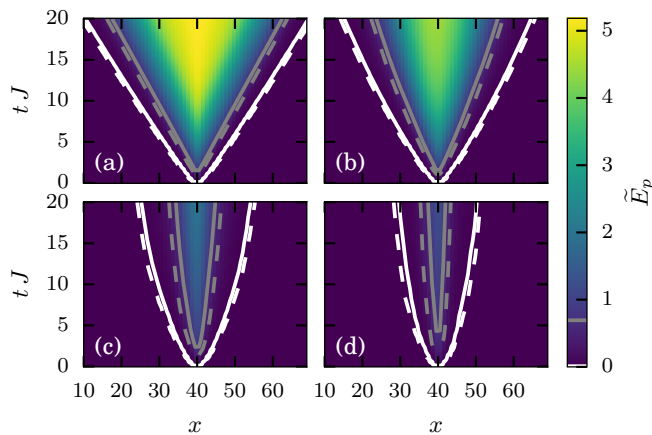


FIG. 4. Optimized entanglement \tilde{E}_p in the state $e^{-itH} S_{L/2}^+ |\psi_0\rangle$ for the Heisenberg model (4) with disorder strength (a) $W = 0$, (b) $W = J$, (c) $W = 3J$ and (d) $W = 5J$, each averaged over 30 disorder realizations. The white and grey solid lines show the contour for the onset of finite values at a threshold of 0.01 and $\log(2)$. The dashed lines shows contours for the same threshold when backward time evolution is used.

Fig. 3(a) compares the resulting entanglement for no disentangling ($U_{\text{anc}} = \mathbb{1}$), backward time evolution ($U_{\text{anc}} = e^{itH}$), and the optimized disentangler ($U_{\text{anc}} = U_{\text{disent}}$). Note that for $\beta = 0$ backward time evolution is equivalent to the Heisenberg evolution of $S_{L/2}^+$. The maximum of the entropy over different bonds (i.e., cuts for the bipartitions) grows roughly linear in all three cases, yet with very different prefactors. As observed before, the growth is spatially almost uniform in the case $U_{\text{anc}} = \mathbb{1}$, while both the backward time evolution and our optimized algorithm develop entropy only within a causal “light-cone”, leading to a significant reduction of the mean entanglement. Fig. 3(b) compares the growth of the required MPS bond dimension when the truncation error is kept fixed. Unfortunately, both backward time evolution and the optimized disentangler require a slightly higher maximal bond-dimension close to where $S_{L/2}^+$ was applied. This apparent contradiction of a larger bond dimension despite a lower entropy can be understood from the fact that entropy has large weight on the largest Schmidt values, but the required bond dimension is determined by the decay of Schmidt values in the tail. Indeed, we show in the inset of Fig. 3(b) that the optimization leads to a reduction in the first few Schmidt values accompanied by a slightly longer tail of small Schmidt values compared to $U_{\text{anc}} = \mathbb{1}$. Nevertheless, the tail decays faster than with backward time evolution.

As a second example, we consider the $S = 1/2$ Heisenberg chain with disordered z -directed field,

$$H = J \sum_{i=1}^{L-1} \vec{S}_i \cdot \vec{S}_{i+1} - \sum_{i=1}^L h_i^z S_i^z, \quad (4)$$

where h_i^z is chosen uniformly in the interval $[-W, W]$. This model has been established as a standard model in the study of many body localization (MBL) [28–30] in one dimension. Numerically a localization transition was found to occur at $W_c \approx 3.5J$ [31, 32]. Fig. 3(c) again compares the entanglement growth of $|S_{L/2}^+(t, \beta)\rangle$ for the three choices of U_{anc} in the clean Heisenberg chain, $W = 0$. While the entropy grows linearly when no disentangler is used, the integrability of the Heisenberg chain and the presence of S^z conservation restricts the entanglement of time evolved local operators in the Heisenberg picture (here the “backward” evolution) to $S(t) \propto \log(t)$ [33]. Our results are compatible with the same $S(t) \propto \log(t)$ scaling when optimized, again with a smaller prefactor. In the MBL phase, Fig. 3(d), even $U_{\text{anc}} = \mathbb{1}$ displays only a logarithmic entanglement growth, which is a characteristic feature of the MBL phase [34–37].

Next we focus on the spatial spread of the entanglement in $S_{L/2}^+ |\psi_0\rangle$ when using the optimized disentangler, tracking $S_{LL'}$ as a function of time t and bipartition bond x , shown in Fig. 4. In the thermalizing regime, at small W , Fig. 4(a) and (b), we observe the expected linear light-cone spreading [38]. Deep in the MBL phase, Fig. 4(d), we find a qualitatively different spreading which is compatible with a logarithmic light-cone. This is as expected from a generalized Lieb-Robinson bound $\| [A_i(t), B_j] \| \leq cte^{\frac{|i-j|}{2\xi}}$, where ξ is the localization length and $c > 0$ some constant [39, 40]. At intermediate disorder, near the MBL transition, we observe a sub-linear spreading of the entanglement. Although there are extended eigenstates in this region, the system is expected to be subdiffusive and exhibits only slow transport on very long time scales (inaccessible to our numerics) [41–44]. Since the backward time evolution already reduces $S_{LL'}$ to a zero (up to exponentially small corrections) outside of the light cone, it is not surprising that the contours of the onset are nearly unchanged compared to our optimized case.

Conclusions. We introduced an MPS based method to find a unitary U_{anc} acting on the ancilla DoF of a purification state, which reduces the entanglement both in equilibrium and during real time evolution, at a similar cost to the TEBD algorithm. At low temperatures, the optimized entanglement entropy \tilde{E}_p is half as large as in the TFD state, providing evidence that the algorithm actually finds the entanglement of purification E_p . We find a maximum of \tilde{E}_p at intermediate β , but leave the investigation of its behavior with Hamiltonian parameters for future work. During real-time evolution, the entanglement is significantly reduced both compared to $U_{\text{anc}} = \mathbb{1}$ and backward time evolution. In the clean Heisenberg chain, \tilde{E}_p shows a linear light-cone structure, which turns to a logarithmic spreading in the MBL phase (at large disorder). The minimization of the entangle-

ment is, however, not directly accompanied by a reduction of the required bond dimensions, as it leads to a larger tail of small Schmidt values. This limitation might be overcome by another choice of local disentangler.

Acknowledgments. We acknowledge useful discussions with Leon Schoonderwoerd. This work was partially supported by the ERC Starting Grant No. 679722. FP acknowledges the support of Research Unit FOR 1807 through grants no. PO 1370/2-1, and the Nanosystems Initiative Munich (NIM) by the German Excellence Initiative.

* E-mail: johannes.hauschild@tum.de

- [1] M. Fannes, B. Nachtergaele, and R. F. Werner, *Commun. Math. Phys.* **144**, 443 (1992), arXiv:9504002 [cond-mat].
- [2] M. B. Hastings, *Phys. Rev. B* **73**, 085115 (2006), arXiv:0508554 [cond-mat].
- [3] U. Schollwöck, *Ann. Phys. (N. Y.)* **326**, 96 (2011), arXiv:1008.3477.
- [4] F. Verstraete and J. I. Cirac, arXiv:cond-mat/0407066 (2004), arXiv:0407066 [cond-mat].
- [5] S. R. White, *Phys. Rev. Lett.* **69**, 2863 (1992).
- [6] G. Vidal, *Phys. Rev. Lett.* **93**, 40502 (2004), arXiv:0310089 [quant-ph].
- [7] A. J. Daley, C. Kollath, U. Schollwöck, and G. Vidal, *J. Stat. Mech. Theory Exp.* **2004**, P04005 (2004), arXiv:0403313 [cond-mat].
- [8] S. R. White and A. E. Feiguin, *Phys. Rev. Lett.* **93**, 76401 (2004), arXiv:0403310 [cond-mat].
- [9] T. Barthel, arXiv:1708.09349 (2017), arXiv:1708.09349.
- [10] G. G. Vidal, *Phys. Rev. Lett.* **91**, 147902 (2003), arXiv:0301063 [quant-ph].
- [11] S. R. White, *Phys. Rev. Lett.* **102**, 190601 (2009), arXiv:0902.4475.
- [12] E. M. Stoudenmire and S. R. White, *New J. Phys.* **12**, 055026 (2010), arXiv:1002.1305.
- [13] M. Berta, F. G. S. L. Brandao, J. Haegeman, V. B. Scholz, and F. Verstraete, arXiv:1709.07423 (2017), arXiv:1709.07423.
- [14] F. Verstraete, J. J. García-Ripoll, and J. I. Cirac, *Phys. Rev. Lett.* **93**, 207204 (2004), arXiv:0406426 [cond-mat].
- [15] T. Barthel, U. Schollwöck, and S. R. White, *Phys. Rev. B* **79**, 245101 (2009), arXiv:0901.2342.
- [16] C. Karrasch, J. H. Bardarson, and J. E. Moore, *Phys. Rev. Lett.* **108**, 227206 (2012), arXiv:1111.4508.
- [17] T. Barthel, *New J. Phys.* **15**, 073010 (2013), arXiv:1301.2246.
- [18] B. M. Terhal, M. Horodecki, D. W. Leung, and D. P. DiVincenzo, *J. Math. Phys.* **43**, 4286 (2002), arXiv:0202044 [quant-ph].
- [19] N. Schuch, M. M. Wolf, F. Verstraete, and J. I. Cirac, *Phys. Rev. Lett.* **100**, 030504 (2008), arXiv:0705.0292.
- [20] E. Leviatan, F. Pollmann, J. H. Bardarson, and E. Altman, arXiv:1702.08894 (2017), arXiv:1702.08894.
- [21] C. D. White, M. Zaletel, R. S. K. Mong, and G. Refael, arXiv:1707.01506 (2017), arXiv:1707.01506.
- [22] J. Haegeman, J. I. Cirac, T. J. Osborne, I. Pizorn, H. Verschelde, and F. Verstraete, *Phys. Rev. Lett.* **107**, 070601 (2011), arXiv:1103.0936.
- [23] M. P. Zaletel, R. S. K. Mong, C. Karrasch, J. E. Moore, and F. Pollmann, *Phys. Rev. B* **91**, 165112 (2015), arXiv:1407.1832.
- [24] C. Karrasch, J. H. Bardarson, and J. E. Moore, *New J. Phys.* **15**, 083031 (2013), arXiv:1303.3942.
- [25] G. Evenbly and G. Vidal, *J. Stat. Phys.* **157**, 931 (2014), arXiv:1312.0303.
- [26] T. Takayanagi and K. Umemoto, (2017), arXiv:1708.09393.
- [27] P. Nguyen, T. Devakul, M. G. Halbasch, M. P. Zaletel, and B. Swingle, (2017), arXiv:1709.07424.
- [28] D. M. Basko, I. L. Aleiner, and B. L. Altshuler, *Ann. Phys. (N. Y.)* **321**, 1126 (2006), arXiv:0506617 [cond-mat].
- [29] I. V. Gornyi, A. D. Mirlin, and D. G. Polyakov, *Phys. Rev. Lett.* **95**, 206603 (2005), arXiv:0506411 [cond-mat].
- [30] D. A. Abanin and Z. Papić, *Ann. Phys.* **529**, 1700169 (2017), arXiv:1705.09103.
- [31] A. Pal and D. A. Huse, *Phys. Rev. B* **82**, 174411 (2010), arXiv:1010.1992.
- [32] D. J. Luitz, N. Laflorencie, and F. Alet, *Phys. Rev. B* **91**, 081103 (2015), arXiv:1411.0660.
- [33] D. Muth, R. G. Unanyan, and M. Fleischhauer, *Phys. Rev. Lett.* **106**, 077202 (2011), arXiv:1009.4646.
- [34] J. H. Bardarson, F. Pollmann, and J. E. Moore, *Phys. Rev. Lett.* **109**, 1 (2012), arXiv:1202.5532.
- [35] M. Žnidarič, T. Prosen, and P. Prelovšek, *Phys. Rev. B* **77**, 064426 (2008), arXiv:0706.2539.
- [36] R. Vosk and E. Altman, *Phys. Rev. Lett.* **110**, 067204 (2013), arXiv:1205.0026.
- [37] M. Serbyn, Z. Papić, and D. A. Abanin, *Phys. Rev. Lett.* **110**, 260601 (2013), arXiv:1304.4605.
- [38] H. Kim and D. A. Huse, *Phys. Rev. Lett.* **111**, 127205 (2013), arXiv:1306.4306.
- [39] I. H. Kim, A. Chandran, and D. A. Abanin, arXiv:1412.3073 (2014), arXiv:1412.3073.
- [40] D.-L. Deng, X. Li, J. H. Pixley, Y.-L. Wu, and S. Das Sarma, *Phys. Rev. B* **95**, 024202 (2017), arXiv:1607.08611.
- [41] K. Agarwal, S. Gopalakrishnan, M. Knap, M. Müller, and E. Demler, *Phys. Rev. Lett.* **114**, 160401 (2015), arXiv:1408.3413.
- [42] A. Chandran, A. Pal, C. R. Laumann, and A. Scardicchio, *Phys. Rev. B* **94**, 144203 (2016), arXiv:1605.00655.
- [43] D. J. Luitz, N. Laflorencie, and F. Alet, *Phys. Rev. B* **93**, 1 (2016), arXiv:1511.05141.
- [44] D. J. Luitz and Y. B. Lev, *Ann. Phys.* **529**, 1600350 (2017), arXiv:1610.08993.
- [45] M. A. Nielsen and I. L. Chuang, *Quantum Computation and Quantum Information* (Cambridge University Press, 2002).
- [46] S. Singh, R. N. C. Pfeifer, and G. Vidal, *Phys. Rev. A* **82**, 050301 (2010), arXiv:0907.2994.
- [47] K. Hyatt, J. R. Garrison, and B. Bauer, *Phys. Rev. Lett.* **119**, 140502 (2017), arXiv:1704.01974.

Disentangling algorithm

Here, we provide details of the algorithm used to identify an optimal unitary U_{disent} (acting on \mathcal{H}^Q) which minimizes the entanglement entropy of a quenched purified

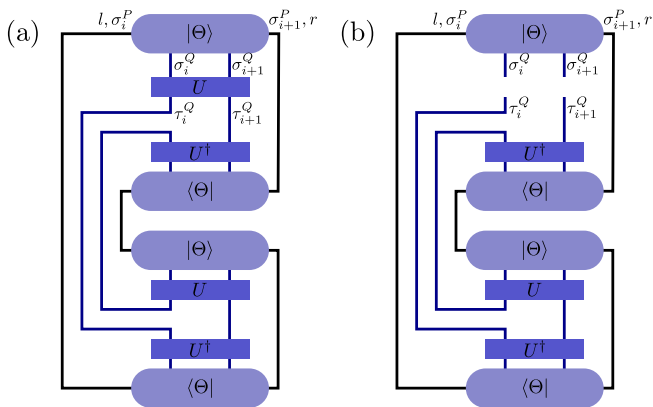


FIG. 5. (a) Tensor network for $Z_2(U, \Theta)$. (b) Effective environment $E_2(U, \Theta)$ such that $Z_2(U, \Theta) = \text{Tr}(U E_2(U, \Theta))$.

state. During real-time evolution, we perform the optimization at each iteration step of the TEBD algorithm. The TEBD algorithm [6] is based on a Trotter decomposition of e^{-itH} into two-site unitaries $e^{-i\delta_t H_{i,i+1}}$ as illustrated in Fig. 1(b). These unitaries are applied to the physical indices of the effective two-site wave function

$$|\Theta\rangle = \sum_{\substack{\sigma_i^P, \sigma_i^Q, l \\ \sigma_{i+1}^P, \sigma_{i+1}^Q, r}} \Theta_{l,r}^{\sigma_i^P, \sigma_i^Q, \sigma_{i+1}^P, \sigma_{i+1}^Q} |l\rangle |\sigma_i^P \sigma_i^Q\rangle |\sigma_{i+1}^P \sigma_{i+1}^Q\rangle |r\rangle,$$

where $|l\rangle$ (and $|r\rangle$) label a basis consisting of Schmidt states to the left of site i (and right of site $i+1$, respectively). In our algorithm, we disentangle the two-site wave function right after each trotter step using a unitary acting on the auxiliary space, such that U_{disent} is gradually build up by two-site unitaries, as depicted in Fig. 1(c). Similar as for the MERA [25] the two-site disentangler can be found iteratively using the polar decomposition, as explained in the following.

The goal is to find a two-site unitary $U = U_{\sigma_i^Q, \sigma_{i+1}^Q}^{\tau_i^Q, \tau_{i+1}^Q}$ (i.e., acting in \mathcal{H}^Q) which minimizes the entanglement of $U|\Theta\rangle$. We chose to minimize the second Rényi entropy $S_2(U|\Theta) = -\log \text{Tr}(\rho_{LL'}^2)$, where $\rho_{LL'}$ is the reduced density matrix $\rho_{LL'} = \text{Tr}_{\sigma_{i+1}^P, \tau_{i+1}^Q, r}(U|\Theta)\langle\Theta|U)$ [45]. In contrast to the von-Neumann entropy, the second Rényi entropy is readily expressed as $S_2(U|\Theta) = -\log(Z_2)$ with the tensor network Z_2 depicted in Fig. 5(a); Z_2 is to be maximized. We solve this non-linear optimization problem iteratively: in the n -th iteration, we consider one U_{n+1} formally as independent of the other U_n and write $Z_2(U_{n+1}, U_n, \Theta) = \text{Tr}(U_{n+1} E_2(U_n, \Theta))$, where the network for $E_2(U_n, \Theta)$ is shown in Fig. 5(b). It is easy to see that the unitary U_{n+1} maximizing this expression is given by a polar decomposition of $E_2(U_n, \Theta)$, in other words we set $U_{n+1} := YX^\dagger$ where X and Y are obtained from a singular value decomposition of $E_2(U_n, \Theta) = XAY^\dagger$. The unitary minimizing $Z_2(U, \Theta)$ is then a fixed point

U_* of this iteration procedure. As a starting point of the iteration, one can choose the identity $U_1 := \mathbb{1}$. At later times, one can also use the result of U_n from previous iterations (for the same time step and at the same bond) as initial guess for the next disentangler, which reduces the number of necessary iterations in many cases.

Since this iteration is based on a descent, it tends to go into local minima within the optimization space. To find the global optimum, we can perform multiple iterations in parallel: one starting from the identity, and others starting from initially random unitaries (chosen from the circular unitary ensemble). From the unitaries obtained by the parallel iterations, we choose the one with the smallest final entropy.

The disentangler U_n obtained by the above procedure preserves the quantum numbers of symmetries in the Hamiltonian, at least if the initial guess U_0 preserves them. In the presence of such a symmetry one should choose U_0 accordingly to avoid an artificial build-up of entanglement. In our case, we exploited the S^z conservation in the Heisenberg chain (4) to reduce the computational cost in the tensor contractions and singular value decompositions [46].

Global disentangling. In contrast to the real-time evolution, the Trotter gate $e^{-\delta_\beta H_{i,i+1}}$ in imaginary time evolution is non-unitary. Thus, it can change the Schmidt values and thus generate entanglement on sites it does not even act on, which creates the necessity for a more global scheme of disentangling than the one presented for the real-time evolution. We suggest to perform the imaginary time evolution as usual (with $U_{\text{anc}} = \mathbb{1}$) and to disentangle only after each n^{th} time-step with one of the two schemes presented in the following: (i) Apply disentanglers over groups of multiple sites, e.g., we can disentangle the wavefunction of four sites. (ii) We disentangle strongly entangled pairs of spins which we can identify by calculating the pairwise mutual information [47].

Disentangling over multiple sites. It is straightforward to generalize the two-site disentangling to multiple sites by grouping multiple sites – at the cost of a scaling of required computational resources which is exponential in the number of included sites. For example, we can disentangle the wave function of four sites $i, i+1, i+2, i+3$ by grouping each two sites as $(i, i+1)$ and $(i+2, i+3)$ and then using the above described method. As the resulting disentangler can perform arbitrary “on-site” rotations within each group, it is necessary to disentangle the obtained wave function (recursively) within each group. We note that left-right sweeps in the same way as in DMRG appear to be more effective than the decomposition of U_{disent} depicted in Fig. 1(c), even when only two-site gates are applied.

Long-range disentangling Alternatively, we can disentangle the MPS with a method along the lines of Ref. [47]. Here, the idea is to identify pairs of sites with

maximal mutual information as candidates for disentangling. Using swap gates (commonly used for TEBD with longer-range interactions [12]), we bring the two sites next to each other and disentangle them with a two-site disentangler as described above for the real-time evolu-

tion. Yet, we find that this approach is very limited by the fact that the purification can not be disentangled completely (except for $\beta \rightarrow \infty$), such that we fail at some point to identify the next candidate pair to be disentangled.